

Alumina-graphene nanocomposite coatings fabricated by suspension high velocity oxy-fuel thermal spraying for ultra-low-wear

James W. Murray¹, Graham A. Rance², Fang Xu¹, Tanvir Hussain^{1*}

¹Faculty of Engineering, University of Nottingham, Nottingham, NG7 2RD, UK

²Nanoscale and Microscale Research Centre, University of Nottingham, Nottingham, NG7 2RD, UK

Abstract

An alumina coating containing 1 wt.% graphene nanoplatelets (GNPs) is deposited for the first time by suspension high velocity oxy-fuel (SHVOF) thermal spraying - an emerging coating deposition technique. Raman spectroscopy shows the GNPs survive the process albeit with a two-fold increase in the density of defects in the graphitic lattice. Dry-sliding wear testing at a 10 N load yields a two order of magnitude reduction in the specific wear rate for the alumina/GNP composite in comparison to the equivalent pure alumina coating. Testing with varying loads shows that the transition to the severe wear regime is prevented until between 30 and 35 N for the alumina + GNP coating which otherwise occurs between 5 and 7.5 N in the absence of GNPs. A reinforced microstructure, and specifically fracture toughness, explains the improved wear behaviour as opposed to tribofilm formation.

Keywords: graphene nanoplatelets; ceramic matrix composite; nanocomposite; nanoparticles; alumina; wear; SHVOF; thermal spray

*Corresponding author. Tel: +441159513795, email: tanvir.hussain@nottingham.ac.uk, address: Room C55, Coates, University Park, Nottingham, NG7 2RD, UK

1. Introduction

Graphene is a 2D sheet of sp^2 -hybridised carbon atoms linked by strong covalent bonds in a hexagonal network [1]. Graphene exhibits a range of attractive properties, including high mechanical stiffness and fracture toughness, thermal and electrical conductivity [2, 3]. Graphene, much like its 3D analogue, graphite, also has excellent solid lubricant properties [4, 5], showing excellent wear behaviour, including on a single layer of graphene [6]. Graphene nanoplatelets (GNPs), also called multi-layered graphene (MLG), are a form of graphene which comprises a stack of a small number of graphene sheets, approx. 20 layers, with a diameter of 5 μm , with much retention of their single layer properties [7]. GNPs represent a good model for the behaviour and properties of pure graphene, and are desirable given their cheaper production costs in comparison to single layer graphene.

The basis for the incorporation of GNPs and carbon nanotubes (CNTs) into ceramics to form a composite is the mechanical reinforcement properties provided to the material by a small volume of nano-materials possessing higher mechanical properties. Toughening mechanisms for graphene platelets in ceramics include sheet wrapping of smaller particles as well as two and three dimensional crack deflection and crack bridging [8]. Additionally, in the case of graphene and GNPs, their lubricating properties can also be exploited for enhanced tribological performance. GNPs, and other carbon based nanomaterials, such as CNTs, have been incorporated as reinforcements into ceramic materials to form composites with enhanced properties. For example, with only 0.07 wt.% of CNTs, an alumina based CNT composite material fabricated by hot pressing yielded a 50% reduction in dry sliding wear rate, along with an enhanced hardness and fracture toughness of 9 and 27% respectively [9]. A spark plasma sintered silicon nitride material incorporating 3 wt.% GNPs has also been fabricated, with a 56% reduction in dry sliding wear rate [10]. Other work has investigated varying wt.% levels of GNP from 0.5 to 2.0,

in spark plasma sintered GNP/alumina composite [11, 12]. In the case of 1% GNP loading, at room temperature, the effect of toughening was seen via direct observation of the crack deflection around a single GNP after fracture of the material. At room temperature, a minor increase in fracture toughness was observed, however this effect was increased at a cryogenic temperature of 77 K. Other work has reported a 235% increase in fracture toughness of spark plasma sintered silicon nitride/GNP composite [8]. In all such studies, the basic structure of the GNPs or CNTs was retained, despite temperatures up to 1650°C.

Despite carbon nanomaterial based ceramic composites having shown improved properties as the result of bulk manufacturing processes, application of such composites as coatings onto engineering substrates represents a more useful and more economical route to enhancement of part performance. Thermal spraying is a widely industrially used family of coating manufacturing techniques which includes high velocity oxy-fuel (HVOF) spraying, plasma spraying and cold gas dynamic spraying, among others. HVOF, as the most commonly used method, typically uses a powder, which is fed into a combustion flame at pressure and sprayed onto substrates with a thickness of up to 100s of μm , with low porosity and excellent coating bond strength. Flame temperatures can reach 2500-2850 °C [13] depending on the fuel type, allowing materials with high melting points, such as ceramics, to be successfully deposited. An emerging version of HVOF uses fine particulates in suspension, called Suspension High Velocity Oxy-Fuel (SHVOF). SHVOF reduced the particle sizes of feedstock which can be deposited by HVOF. It can also result in a more dense coating, with finer microstructures reflecting the original particle size, in comparison to conventional HVOF. The key advantage of thermal spray processes, such as HVOF, is the high speed of processing, and it is a convenient route for incorporating nanomaterials into engineering products. It is a potentially convenient method for improving performance of engineering components

with a relatively small volume of material compared to that of the bulk component, via the formation of a GNP/ceramic composite.

GNP based composites have not been investigated through a high temperature spraying process, such as HVOF, which are expected to partially or fully melt ceramic feedstock materials. In this case, the survivability of graphene in such high temperatures in the presence of oxygen is not known and hence remains a key question for advancing graphene/ceramic coatings. In the case of cold-spray, the graphene oxide variant has been successfully deposited, although in this case, the much higher temperatures of HVOF and plasma spraying are avoided [14]. CNTs are an example of a nanomaterial which has been successfully deposited by HVOF and plasma spraying. The retention and homogeneous distribution of multi-walled CNTs has been demonstrated in both HVOF and plasma spraying [15, 16]. In the case of plasma spraying of CNTs in a feedstock of an Al-Si alloy, CNTs were observed mostly between splats in the coating structure. Critically, there was no evidence of reaction of CNTs with oxygen or aluminium despite the higher processing temperatures [15]. Given the promising mechanical properties of GNP based ceramic composites, investigation of their structure after spraying by HVOF is necessary to promote their adoption as a coating material.

Here, we investigate the addition of a small weight percentage (1 wt. %) of GNPs to a SHVOF alumina coating and use the dry sliding wear as a means to assess the performance of the composite coating, in comparison to that of a pure alumina one. Alumina is investigated as the primary constituent of the sprayed composite, given its usefulness as a wear resistant coating, with good dry sliding wear properties, low cost and good sprayability by HVOF. Alumina feedstock normally comprises the desirable alpha phase, giving the best wear performance of the various forms of alumina. Given the high temperatures of the HVOF process, it is difficult to retain the alpha phase, and often the gamma phase forms, with poorer wear properties owing to its lower fracture toughness

and hardness [17]. Avoiding the gamma phase requires careful selection of typically lower flame energy parameters, which in turn can exacerbate the prevalence of porosity and hinder coating properties. This study is focused on the improvement of an SHVOF alumina coating with a large percentage of gamma alumina, *via* the addition of GNPs to the feedstock. This coating is sprayed at 101 kW, typical industry standard parameters for this spray setup, which yields better melting, lower porosity and higher bond strength compared to lower power parameters and would be more appropriate for engineering application. A feedstock was prepared by dispersing GNPs in a suspension of alpha alumina, prior to SHVOF spraying onto stainless steel substrates. The wear performance is characterised in comparison to an equivalent alumina coating without GNPs, and critically, the distribution and physical state of GNPs before and after spraying is measured by detailed Raman spectroscopic mapping.

2. Experimental

2.1. Feedstock preparation

A suspension was prepared using CR1 alpha alumina powder (Baikowski, France) with a D50 particle size of 1 μm and graphene nanoplatelets (GNP) 6-8 nm thickness and 5 μm average diameter (ABCR product no. AB 304022). 4.75 grams of GNPs were dispersed in 500 ml deionised water using an ultrasonic probe for 50 minutes. The alumina powder suspension, also in deionised water at a concentration of 35 wt.% (474 g in 1380 g of water) was stirred for three hours to ensure the uniformity of the suspension, after which the freshly dispersed GNP mixture was added to the alumina, and the final mixture was further stirred for 30 minutes, after which spraying was performed immediately. The final suspension equated to 1% GNPs by weight and 99% alumina, equating to a solid content of 25.7%, with the remainder deionised water. Figure 1 shows SE images of the nanoplatelets and alumina powder before suspension/mixing.

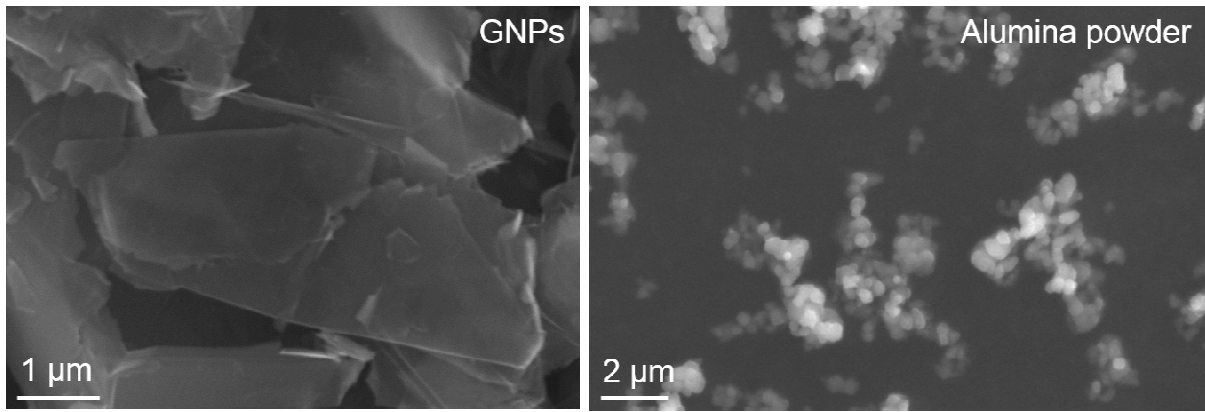


Figure 1 SE images of pure GNPs and pure Alumina powder before suspension in deionised water

2.2. Coating preparation

SHVOF coatings of pure alumina and alumina + 1% by weight GNP were sprayed onto stainless steel substrates with dimensions of 60x25x2 mm. Substrates were grit blasted and cleaned with alcohol before coating. A UTP TopGun HVOF spray system, modified with a 0.3 mm suspension injector diameter was used for spraying. The suspension injector tube has a larger diameter than the powder injector tube and hence it requires a modified gun back-body, a modified gas-fuel mixing chamber and a mixing chamber holder with a larger central hole. Hydrogen fuel, which results in cleaner combustion products, was combusted in a 22 mm long chamber, into which the suspension was fed at a pressure of 3 bar from a mechanically stirred, pressurised chamber. Suspension flow rate was 100 ml/min for all tests. The flow rates of O₂ and H₂ were 306 and 612 l/min respectively, yielding a 101 kW flame power. Substrates were mounted on a rotating carousel at 73 rpm (substrate speed of 1 m/s), while the spray gun was traversed perpendicular to the substrate movement direction, at a speed of 5 mm/s, resulting in an interpass step of 4 mm, until a coating thickness of approximately 60 μm was achieved. Compressed air cooling was applied to the substrates during spraying to prevent overheating. The stand-off distance was fixed as 85 mm for both coatings. A shorter

stand-off distance is used in SHVOF spray to avoid rapid particle deceleration in the flame due to a finer particle size.

2.3. Coating characterisation

Cross-sectional coating analysis was performed after cutting samples using a SiC cutting disk and sequential SiC grinding and diamond polishing with a final grit size of 1 μm . All samples analysed by scanning electron microscopy (SEM) were platinum coated before inspection to provide sufficient electrical conductivity. Microscopy was performed using an FEI XL30 in secondary electron (SE) and back-scattered electron (BSE) modes and Hitachi S-2600 SEM in SE mode for tilted imaging. X-ray diffraction (XRD) was performed with a Bruker D500 using Cu $K\alpha$ radiation, wavelength 0.154 nm, and scanning from 5-120° 2θ values, with a step size of 0.04° 2θ and a step time of 24 s. Raman spectroscopy was performed using a Horiba Jobin Yvon LabRAM HR spectrometer equipped with an automated *xyz* stage (Märzhäuser). Spectra were acquired using a 532 nm laser at 2.5 mW power, a 100 \times objective and a 300 μm confocal pinhole. To simultaneously scan a range of Raman shifts, a 600 lines/mm rotatable diffraction grating along a path length of 800 mm was employed. Spectra were detected using a Synapse CCD detector (1024 pixels) thermoelectrically cooled to -60 °C. Before the spectra collection, the instrument was calibrated using the Rayleigh line at 0 cm^{-1} and a standard Si (100) reference band at 520.7 cm^{-1} . During mapping, spectra were collected between 100 and 3000 cm^{-1} across an area of 24 \times 24 μm with a grid spacing of 1 μm along both the x and y axes, a total of 625 spectra per map. As each individual spectrum was collected for 20 seconds, repeated once in order to automatically remove the spikes due to cosmic rays, the whole map required approximately 7 hours of acquisition time. The height intensity of the D (1190-1470 cm^{-1}), G bands (1480-1700 cm^{-1}) and 2D bands (2600-2800 cm^{-1}) and the corresponding

intensity ratios, $I_D:I_G$ and $I_{2D}:I_G$, were determined within the mapped cross-sectional area. Representative spectra were extracted from the mapped data set, corrected for fluorescence by application of a polynomial baseline subtraction and normalised to the intensity of the G band for comparison. The position and width of spectral features was determined using the Lorentzian peak fitting function in Labspec 6. The penetration of the laser into the samples was determined by performing a z-map and measuring the FWHM of the associated response curve and was found to be ~6 microns.

Fracture surfaces were prepared by gradual bending of the substrate in a vice with the coating attached, yielding fracture surfaces in directions perpendicular, i.e. cross-sectional, and parallel to the top surface. Wear rates were measured by 5 contact profiles of each wear track, taken using a Talysurf CLI 1000 (Taylor Hobson) with a lateral resolution of 0.5 μm . Average cross-sectional area of the profiles was used to calculate total volume worn. Hardness was measured using 10 Vickers indents at a load of 50 gf, chosen to avoid yielding cracks. Fracture toughness was calculated from 10 measurements using Vickers indentation at 200 gf to yield cracks in directions parallel to the coating surface. All indentation work including for hardness and fracture toughness was performed on polished cross-sections prepared with final diamond grit size of 1 μm . The following equation was used from Evans & Charles to calculate fracture toughness [18]:

$$K_{IC} = 0.16 (c/a)^{-1.5} (H_a)^{1/2}$$

Where K_{IC} is fracture toughness in $\text{MPa}\cdot\text{m}^{1/2}$, c is average length of cracks from tips of the Vickers indent (μm), a is the half average length of the diagonal of the Vickers indent (μm), and H is Vickers hardness (MPa) implied from the same indents. No vertical cracks were produced by indentation for the fracture toughness calculation. In

all cases two cracks propagated horizontally, along lamellar boundaries, from the left and right corners. These two values were used to compute the fracture toughness.

Porosity of the coatings was measured using image analysis software ImageJ (NIH, USA) on polished cross-sections of BSE images using a thresholding technique. For each measurement, four images with a field of view of approximately 100 μm by 100 μm was chosen.

2.4. Wear testing

Ball-on-flat dry sliding wear testing was performed with a CETR UMT-2 micro-tribometer (CETR, USA), in reciprocating mode, using a 6.3 mm diameter polished alpha alumina ball counterbody (Dejay Ltd UK). Coatings were worn after sequential polishing using SiC followed by diamond to a final stage of 1 μm grit, yielding a surface roughness prior to wear testing of ~ 0.05 μm Ra. An initial 2 tests were performed at 10 N load given the expected severe wear regime for the alumina sample at this parameter. Further wear tests were performed using a load range from 5-35 N and 10 mm stroke length, (5 mm track length) in order to find the transition points from mild to severe load for both the pure alumina and the alumina + GNP coatings. Sliding speed was 10 mm/s in all tests.

3. Results

3.1. Characterisation of as-sprayed coatings

Based on secondary electron (SE) images of fracture surfaces, GNPs appeared in dimensions close to those of the original raw feedstock. EDX elemental mapping was used to identify carbon, and hence GNPs, given the absence of other carbon sources in the coating. Based on fracture surface imaging, as shown in Figure 2, in both parallel and cross-sectional geometries, GNPs were well distributed, with little evidence of clustering. The orientation of platelets from fracture surface imaging however cannot be determined in either orientation.

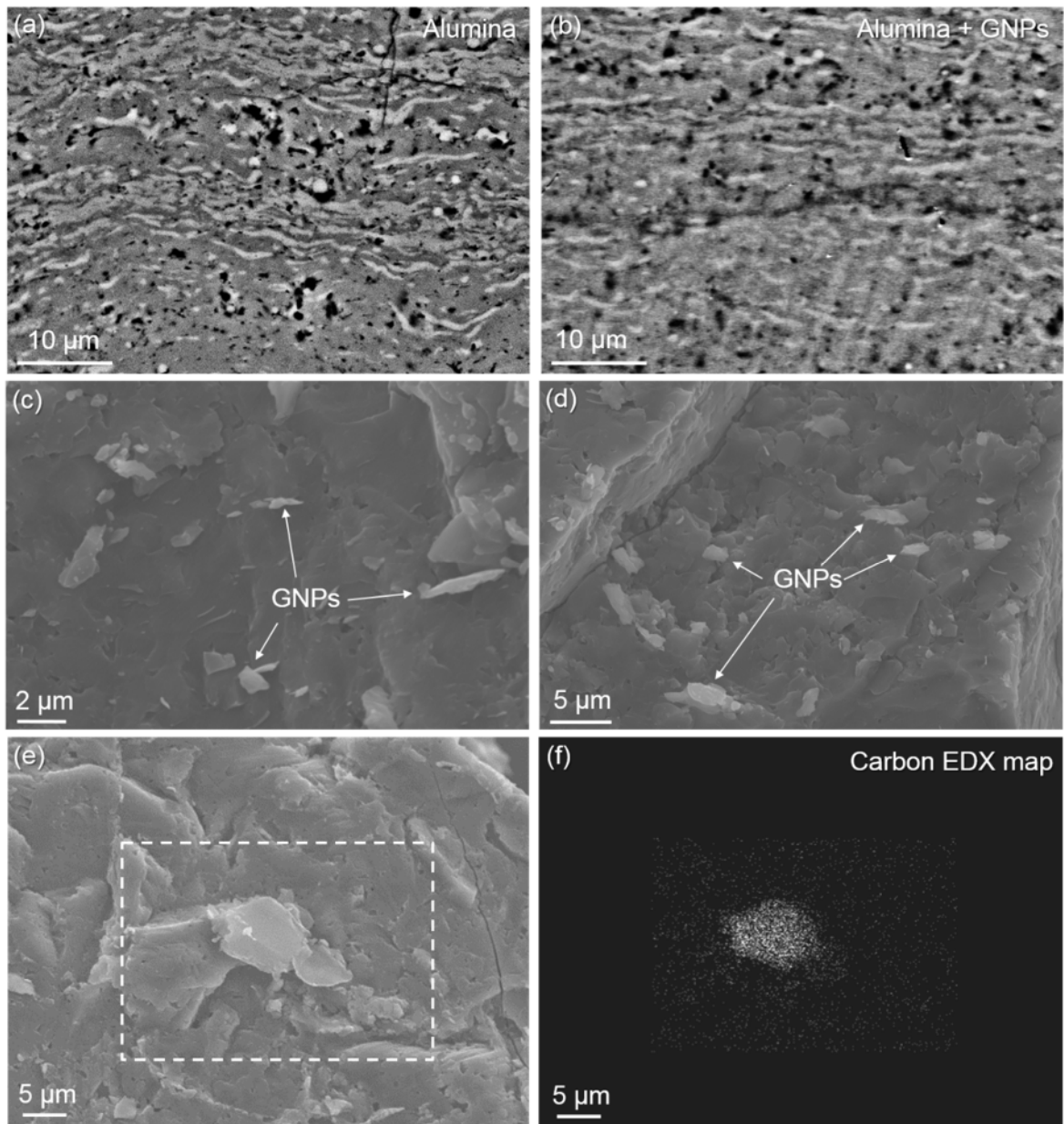


Figure 2 SEM images of (a) alumina coating cross-section without GNP, (b) alumina + GNP coating cross-section, and fracture surfaces (c) perpendicular to top surface of alumina + GNP and (d) parallel to the top surface of alumina + GNP. Numerous GNPs can be seen in various orientations. (e) SE image and (f) EDX mapping of a single GNP on a fracture surface showing the presence of elemental carbon in the location of a topological feature assumed to correspond to a GNP.

To (i) confirm and spatially locate the incorporation of GNPs into the coating subsequent to thermal spraying and (ii) determine the potential impact of thermal spraying on the structural properties of the GNP in the coating, Raman spectroscopic mapping was performed on a polished cross-section of the alumina + GNP coating. The Raman spectrum of GNPs is dominated by three spectroscopic features: the G band – a high frequency E_{2g} optical phonon observed in all forms of nanoscale carbon at $\sim 1580\text{ cm}^{-1}$; the D band – an A_{1g} breathing mode of six-atom rings, requiring a defect for its activation, found in defective and nanocrystalline graphite at $\sim 1350\text{ cm}^{-1}$; and the 2D band (sometimes referred to in the literature as the G' band) – the second order of the D band at $\sim 2700\text{ cm}^{-1}$ [19]. Individual Raman spectra were collected at $1\text{ }\mu\text{m}$ intervals from an area $24\text{ x }24\text{ }\mu\text{m}$ and the variation in the intensity of both D, G and 2D bands in the sprayed coating (Figure 3a, b and d) correlated with spatial location.

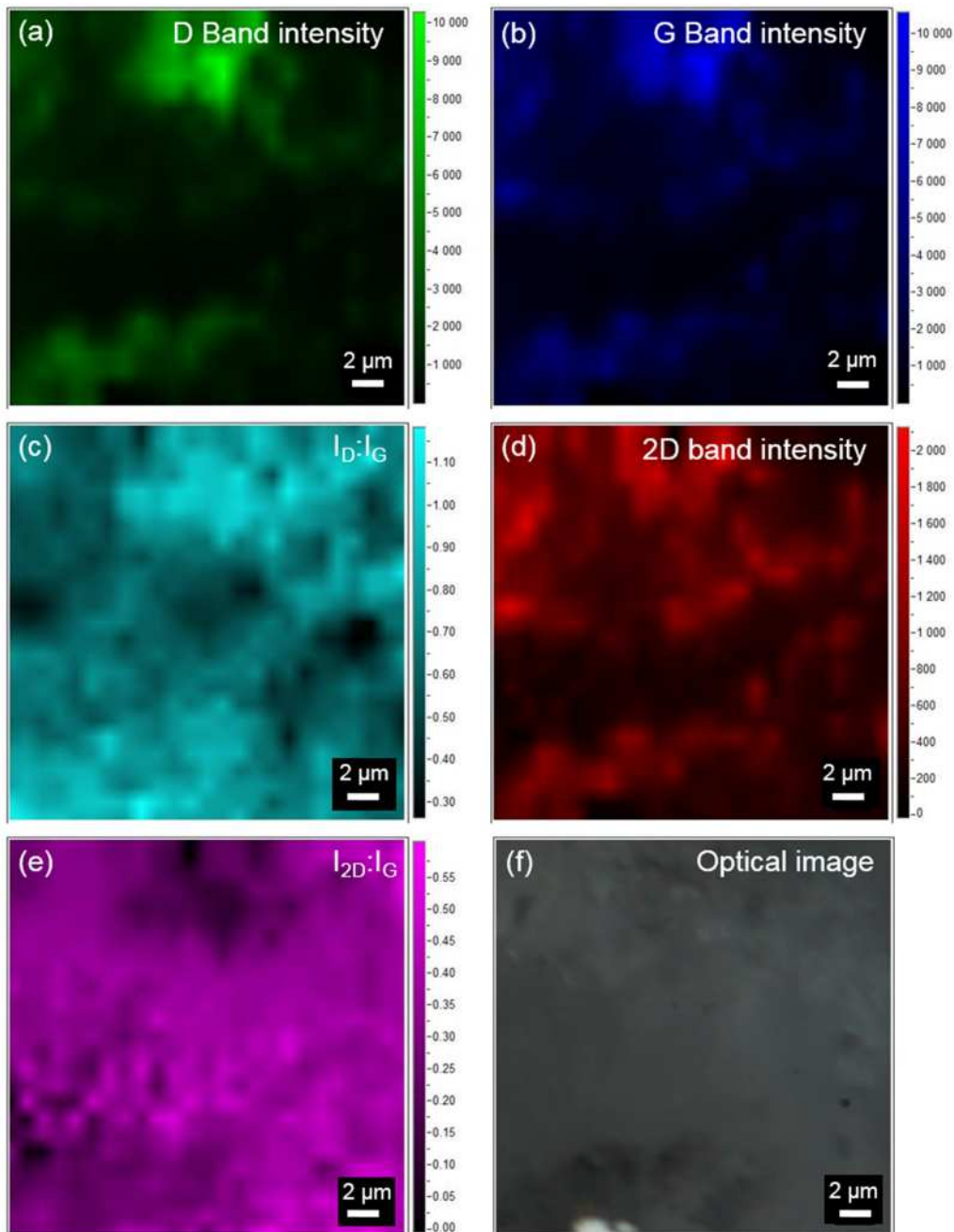


Figure 3 (a-e) Raman spectroscopic maps and (f) optical image of the cross-section of the sprayed alumina-GNP coating, indicating how (a) the intensity of the D band ($1190\text{-}1470\text{ cm}^{-1}$), (b) the intensity of the G band ($1480\text{-}1700\text{ cm}^{-1}$), (c) the intensity ratio of the D and G bands, (d) the intensity of the 2D band ($2600\text{-}2800\text{ cm}^{-1}$) and (e) the intensity ratio of the 2D and G bands vary as a function of spatial location.

Brighter colours in (a), (b) and (d) correspond to a greater intensity (as peak height) of the D, G and 2D bands respectively, consistent with higher concentration of GNP at these locations. Brighter colours in (c) correspond to a greater intensity

ratio of D and G bands, reflecting lower structural purity (higher defectiveness) of the GNP within the sprayed coating.

The D, G and 2D band maps confirm that GNPs are present throughout the mapped region of the cross-section of the coating, with some evidence of clustering into 5-10 μm aggregates observed (bright colouration in the associated maps). As the experimentally-determined penetration of the laser into the sample under the applied experimental conditions is approximately $\sim 6 \mu\text{m}$, the differences in the observed intensity of bands in the lateral directions is likely to reflect the relative location of GNP in the axial direction (i.e. depth); however, in all recorded spectra, the presence of GNP is confirmed.

The ratio of D and G band intensities ($I_D: I_G$) is often used to quantify defectiveness in graphene related systems, such as GNP, and is known to vary with the amount of disorder (deviation from an ideal sp^2 -hybridised carbon lattice due to the incorporation of point defects, such as resonant scatterers and substitutional atoms) within a given graphitic plane. Interestingly, the $I_D: I_G$ map (Figure 3c) shows significant variation in the intensity ratio of D and G bands with spatial location, ranging from 0.27- 1.17. It is important to note however that $I_D: I_G$ was also found to vary between 0.06- 0.54 and 0.01- 0.47 in analogous spectroscopic maps of the unprocessed GNP powder and a deposited GNP dispersion subsequent to ultrasonication respectively, reflecting the dispersity of structural features common within nanoscale carbon materials and thus the necessity for spectroscopic mapping and careful, statistical treatment of the afforded spectral data (Table 1 and Figure 4b).

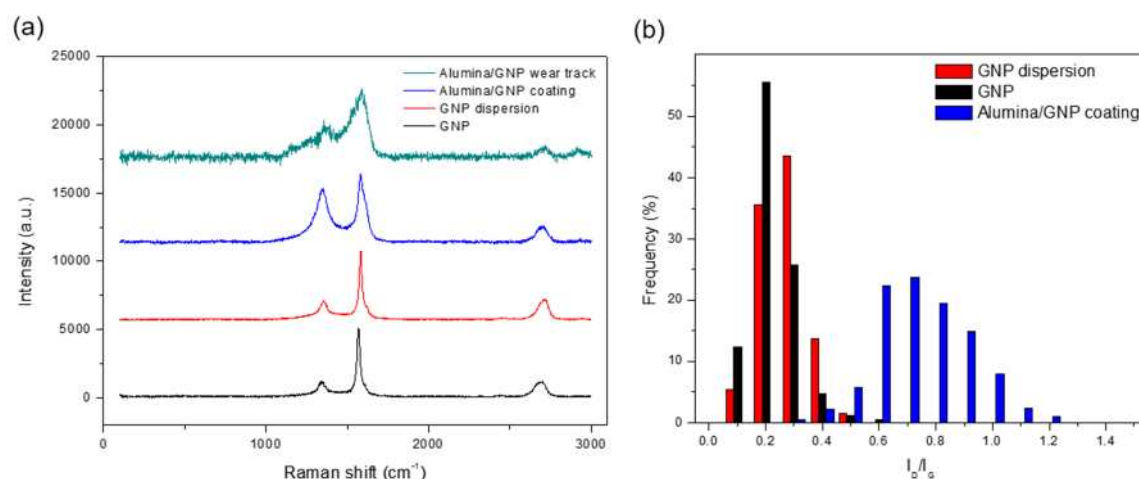


Figure 4 (a) Mean Raman spectra of the unprocessed GNP, dispersed GNP prior to spraying, GNP within the alumina sprayed coating, and spectra from the wear track of the 10 N Alumina/GNP sample extracted from the corresponding spectral maps. Spectra have been baseline corrected for fluorescence, normalised to the intensity of the G band for ease of comparison and shifted on the y-axis for clarity.

(b) The distribution of $I_D:I_G$ extracted from the mapped regions of pure GNP, dispersed GNP and the sprayed coating.

Table 1 Correlated $I_D:I_G$ and $I_{2D}:I_G$ values for the GNP-containing materials.

	$I_D:I_G$		L_D / nm	$I_{2D}:I_G$	
	mean	range		Mean	range
GNP powder	0.18±0.08	0.06-0.54	28.5	0.23±0.02	0.17-0.47
GNP dispersion	0.22±0.08	0.01-0.47	25.7	0.21±0.04	0.09-0.34
Alumina + GNP coating	0.70±0.16	0.27-1.17	14.4	0.32±0.09	0.01-0.60

Comparison of the mean Raman spectra of GNP (Figure 4a) extracted from the maps of the sprayed coating and the unprocessed GNP respectively clearly demonstrate the

differences in structural ordering in the GNP. In addition to an increase in the mean $I_D:I_G$ ratio from 0.18 ± 0.08 to 0.70 ± 0.16 (Figure 4b), corresponding to a 50 % reduction in distance between defects, L_D , from 28.5 to 14.4 nm according to $L_D = 1.8 \times 10^{-9} \lambda^4 \cdot (I_D:I_G)^{-1}$ [21], a ~2-fold enhancement in the width of the D (from 54 to 92 cm^{-1}) and G bands (from 22 to 40 cm^{-1}) further supports the formation of a broader range of more structurally defective GNP subsequent to thermal spraying. For perspective, a fully disordered graphene layer may have an $I_D:I_G$ ratio of over 3 [19]. An apparent shift in the position of the G band subsequent to spraying is associated with the activation of the D' band at $\sim 1620 \text{ cm}^{-1}$, a further indicator of the formation of structural defects. It is important to note that no significant differences in the mean Raman spectra of the unprocessed GNP powder and the deposited GNP dispersion subsequent to ultrasonication were noted. This indicates that is the thermal spraying procedure, rather than the dispersion stage, that results in differences in the structural ordering within the GNP, as has been observed previously in analogous studies on the incorporation of CNTs in alumina by HVOF [22]. Given that the feedstock is passed through a combustion chamber in the presence of a combusted fuel at elevated temperatures, increases in the number and changes in the nature of structural defects in nanocarbons are likely, including the incorporation of substitutional atoms through chemical functionalisation, and may account for the increase in $I_D:I_G$ and broadening of spectral features of the GNPs after spraying.

Interestingly, there is no change in the intensity (relative to the G band), position or width of the 2D band subsequent to thermal spraying, indicating that this treatment does not lead to changes to the number and orientation of graphitic layers within a given stack [19]. Thus, whilst moderate intralayer disorder has been introduced, the afforded GNP within the coating retains much of the structural integrity and thus functional properties of the unprocessed parent material.

XRD was performed on the as-sprayed alumina and alumina + GNP coatings in order to confirm that addition of GNPs does not affect the alumina based microstructure of the coating, the results of which are shown in Figure 5. An almost identical microstructure was observed for both coating types, consisting of a majority of gamma alumina with some small alpha peaks. Both coatings contained a considerable amorphous content, with crystallinity calculated *via* Rietveld refinement to be ~26%, with 95% of crystalline material composed of gamma alumina, and 3% attributed to alpha, and a minor amount to underlying steel substrate material detected. Signal for GNPs was not detected by XRD, explained by the low content in the coating.

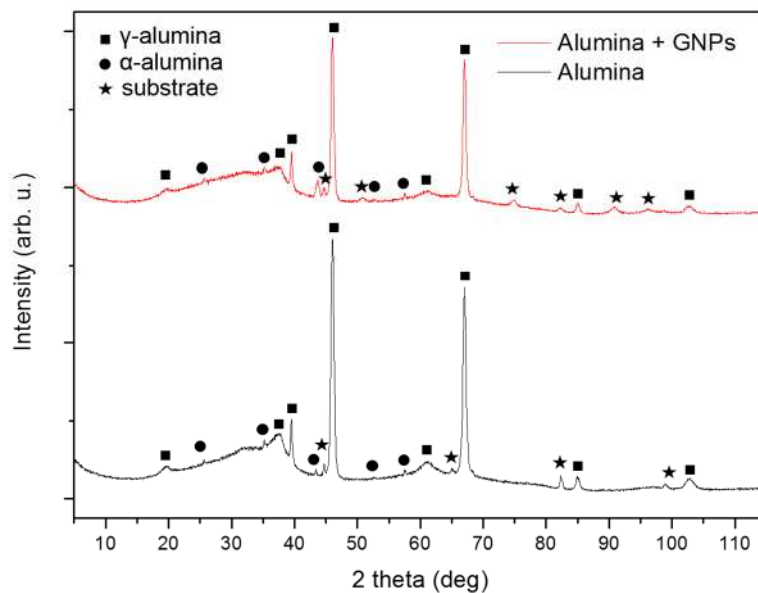


Figure 5 XRD patterns of Alumina and Alumina + GNP coatings, revealing the same alumina- based microstructure with significant amorphous phase. The structure is unchanged by the addition of GNPs, with no evidence of graphene in the pattern, due to low constituent weight %.

3.2. Mechanical properties and porosity

The results of mechanical properties and porosity of the two coating types are shown in Table 2.

Table 2 Hardness and fracture toughness of coatings measured in cross-section, with standard deviations

	Hardness (HV _{0.05})	Fracture toughness (MPa.m ^{1/2})	Porosity (area %)
Alumina	891 ± 225	1.06 ± 0.58	3.53 ± 0.49
Alumina + GNPs	933 ± 198	2.20 ± 2.00	3.13 ± 1.01

Considering the standard deviation of results, hardness was unchanged by the addition of GNPs. The large standard deviation is explained by the mixture of phases present within the coating. A small level of alpha alumina is present in both coatings which is expected to reinforce the material, and therefore it is likely some of the indent interaction volumes include regions containing alpha as well as the softer gamma and the amorphous phase. The large standard deviations seen for the fracture toughness results are also explained by this phenomenon, which is particularly the case here given the larger indent size associated with the 200 gf indentation. Nevertheless, the mean fracture toughness of the alumina + GNP sample is more than doubled in comparison to the pure alumina coating despite the scatter in the results.

Porosity was also measured via image processing analysis of four regions of the coating cross-sections. Considering the error measured in the results, it is not possible to be confident in any reduction in porosity for the sample with the addition of GNPs, despite the slight reduction in mean porosity from ~3.5 to ~3.1%.

3.3. Preliminary wear tests at 10 N

For initial wear tests, a load of 10 N and sliding speed of 10 mm/s, and 4 hours wear time were chosen, as previous work had shown that this parameter caused the coating to enter into a severe wear regime [17]. Hence, these parameters were chosen in order to determine if the GNP reinforcement fundamentally alters the wear mechanism. Two

repeats were performed for each test. Specific wear rates of the wear tracks on coating and counterbodies, based on volume measurement, are shown in Figure 6.

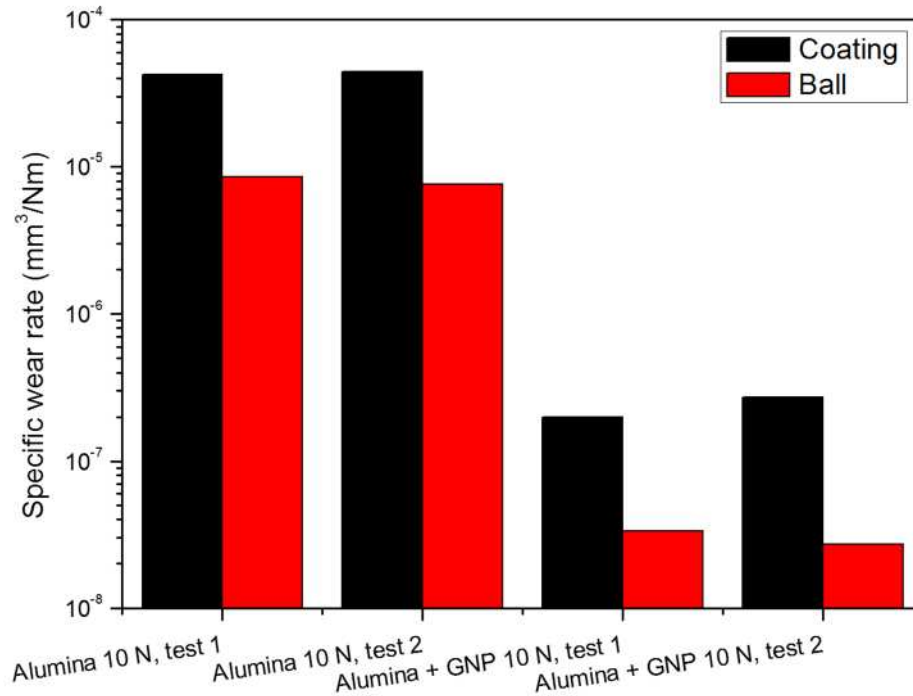


Figure 6 Specific wear rates of alumina and alumina + GNP composite coatings at 10 N load for 4 hours (144 m). A two order of magnitude reduction in wear loss is seen in the alumina/GNP composites.

After 4 hours of wear, the alumina + GNP composite coatings yielded a specific wear rate more than two orders of magnitude lower than the pure alumina coatings, from $\sim 3 \times 10^{-5}$ to $\sim 1-2 \times 10^{-7}$ mm³/Nm. In all cases, the specific wear rate of the counterbody, composed of alpha alumina, was lower than that of the corresponding coating, reflecting the superior performance of the alpha alumina counterbody. Ball wear rates were also reduced by more than two orders of magnitude for the alumina/GNP wear tests. Images of coating wear tracks are shown in Figure 7.

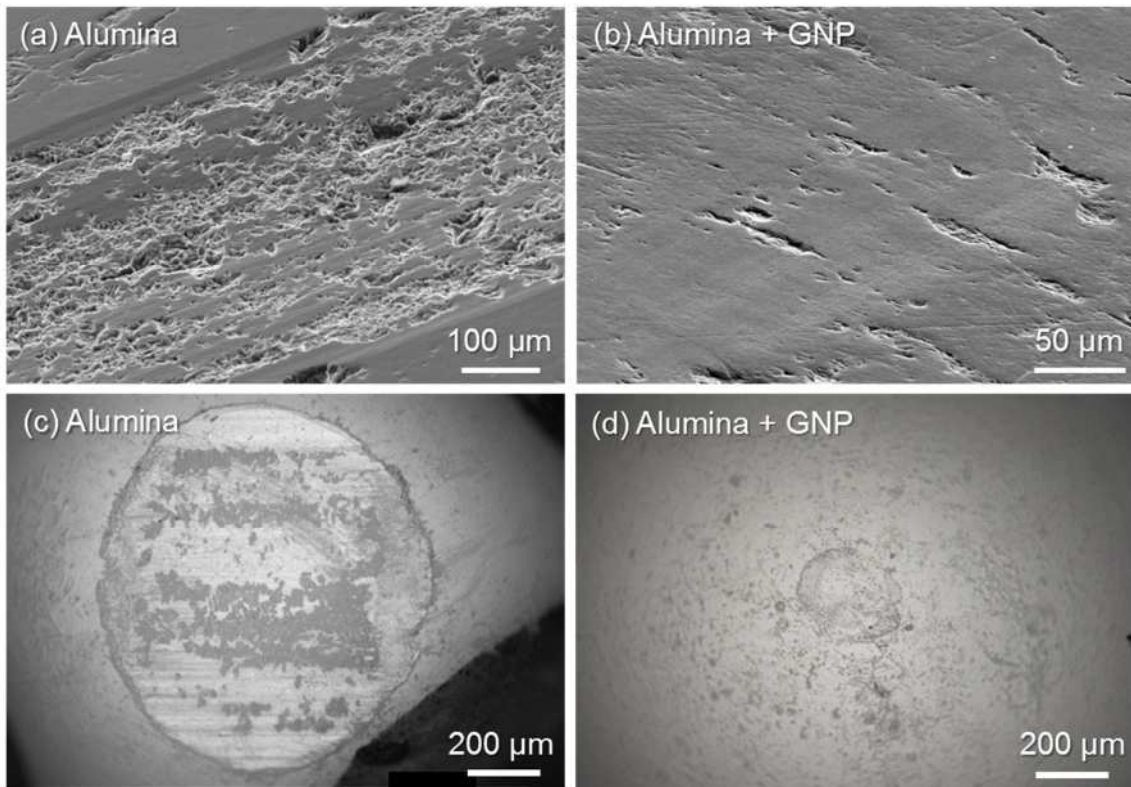


Figure 7 (a) and (b) SEM images of coating wear tracks, and (c) and (d) optical images of counterbody wear spots. Note smaller scale on top right image.

A wear track characteristic of a severe wear regime can be seen on the pure alumina coating (Figure 7 a), characteristic of a brittle fracture mechanism. In contrast, the wear track on the alumina + GNP coating reveals a mild wear mechanism characteristic of a small level of plastic deformation. In Figure 7c and d, wear tracks on the alumina counterbodies worn against the alumina and alumina + GNP coatings respectively are shown. A large wear track with evidence of adhesion of coating material to the track can be seen in (c), whereas, a much smaller wear spot was yielded on the ball worn against the GNP coating. In Figure 8, linear profiles are shown taken across the wear tracks, from which specific wear rate volumes were taken. The alumina coating yielded a ~20 μm deep wear track with a rough topography and clean, sharp track edges. The GNP coating however produced a wear track with a depth on the order of $<1 \mu\text{m}$. Track width was also smaller by a factor of ~5.

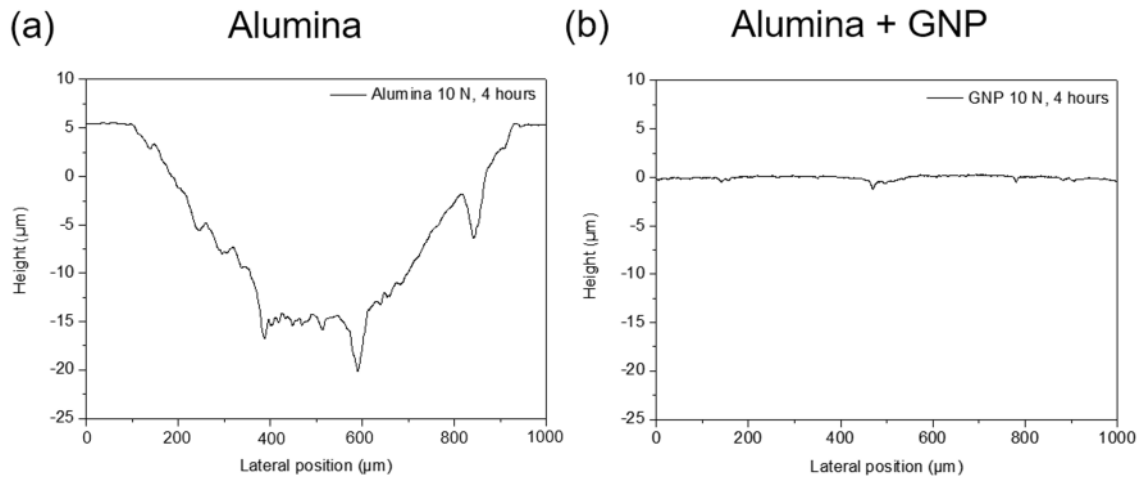


Figure 8 Profiles of wear tracks on the pure and GNP reinforced alumina coatings.

Coefficients of friction for one of each of the two test types can be seen in Figure 9.

Several key differences can be seen between the friction profiles for the two wear tests.

Firstly, an initially rapid increase in friction coefficient to 0.7 was produced in the alumina coating, which then sharply decreased. This can be contrasted with the initial increase to 0.3 which did not reduce again after this point. Secondly after the initial running in period, the alumina coating maintained a slightly higher coefficient of friction compared to the alumina + GNP coating – ~0.45 compared to ~0.35. It should also be noted that the friction behaviour is more erratic for the pure alumina coating, likely reflecting the removal of material and hence change of surface during the test.

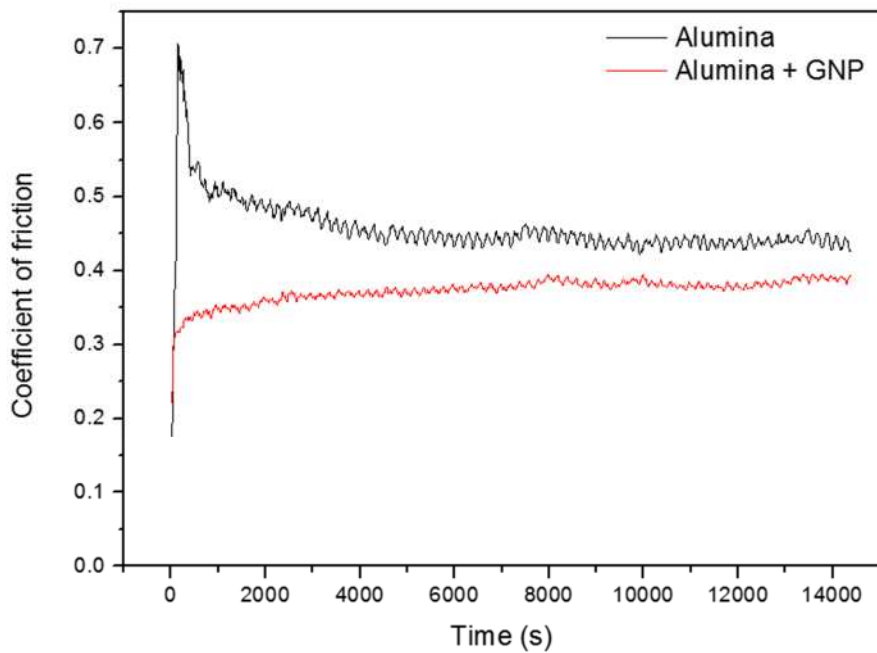


Figure 9 Coefficients of friction against time for alumina and alumina + GNP coating wear tests.

3.4 Determination of mild to severe wear transition

Initial testing at 10 N and 4 hour wear time revealed a two order of magnitude improvement in the specific wear rate with the addition of 1 wt.% GNPs to the alumina coating, *via* the transition to an apparent mild wear mechanism. However, to fully characterise the wear behaviour of the two coatings, and specifically to determine the difference in wear mechanism transition points, wear tests were repeated using a range of loads. Figure 10 shows the specific wear rates for the pure alumina coating at 5 and 7.5 N, and for the alumina + GNP coating at 12.5, 15, 20, 25, 30 and 35 N. All tests were performed for 30 mins, except for the 35 N test which was stopped after 2.5 mins, due to potentially equipment-damaging high friction levels.

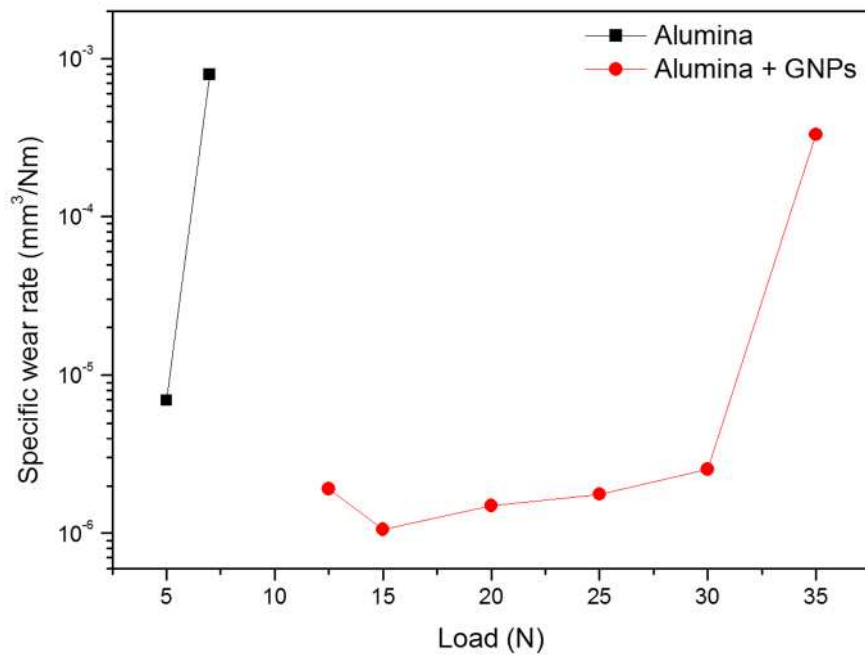


Figure 10 Specific wear rates with and without GNPs, with increasing loads.

Transition to severe wear is between 30 and 35 N for the alumina + GNP composite coating, and between 5 and 7.5 N for the pure alumina coating.

After reducing wear test load on the pure alumina coating to 7.5 N, the wear rate remained high, with a deep wear track and track topography typical of a severe wear regime. Upon reducing to 5 N load, a shallow wear track, with a specific wear rate two orders of magnitude lower than at 7.5 N, indicative of a mild regime was produced, implying the transition for the pure alumina coating between mild and severe wear exists between loads of 5 and 7.5 N. The alumina + GNP coating was then tested with increasing loads. For loads between 12.5 and 30 N, no significant difference in wear track volume was seen, resulting in specific wear rates relatively consistent between these parameters. At 35 N, wear testing resulted in very high friction, and the test was stopped after 2.5 minutes to avoid machine damage. Specific wear rate at 35 N was measured at approximately two orders of magnitude higher than tests between 12.5 and 30 N. The transition point from mild to severe wear for the Alumina + GNP coating was

hence measured to be between 30 and 35 N, hence 4-5 times higher than for the alumina coating.

To explain the shift in transition load, SEM images were taken of the wear track surfaces of 25, 30 and 35 N tests on the alumina + GNP composite coating.

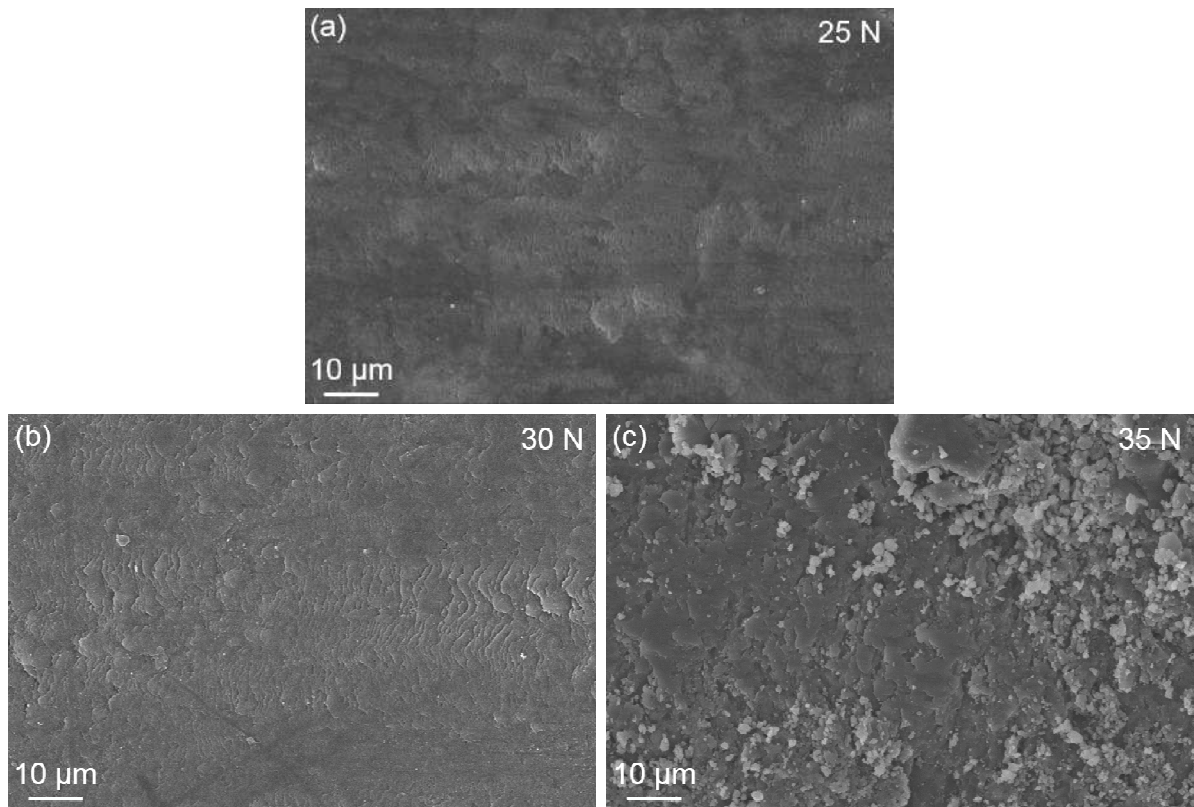


Figure 11 SE images of wear tracks on alumina + GNP composite coating at loads below the transition point to severe wear: (a) 25 N and (b) 30 N, and (c) at a severe wear load of 35 N

At 30 N, a relatively smooth wear track was produced, with grooves characteristic of plastic flow, but with no evidence of intergranular fracture or wear debris. The 25 N wear track showed a similar morphology to the 30 N sample, albeit with smaller grooves indicative of plastic flow, and again no evidence of intergranular fracture. At 35 N load, the wear track is typical of a severe wear regime, with extensive wear debris,

and a rough, pocketed surface characteristic of grain pull out following intergranular fracture. Flat regions characteristic of plastic flow are also present.

Figure 12 shows coefficients of friction for increasing loads for the two coating types. For the pure alumina coating, at 7.5 and 10 N, a rapid initial increase in friction was observed, followed by a gradual decrease towards a steady state coefficient of friction of ~ 0.5 . In contrast, the 5 N sample experienced only a gradual initial increase to ~ 0.3 , followed by a steady but gradually increasing coefficient of friction. For the GNP coating, all tests except at 35 N showed an initial friction increase at a shallower rate than the pure alumina coating at 7.5 and 10 N. The friction coefficient curves of alumina + GNP coatings at lower loads of 12.5- 25 N show noise of ~ 0.5 amplitude which was also observed in the alumina coatings without GNP under 5 N load. This is probably a stick-slip phenomenon occurring during sliding wear. The 35 N coating displayed an immediately sharp rise in friction to ~ 0.7 , at which point the test was stopped. Generally, the mean friction level during wear reflects both the load and the regime of the wear process (i.e. highest for severe wear, lower for mild wear with high load, and lower again for mild wear and low loads).

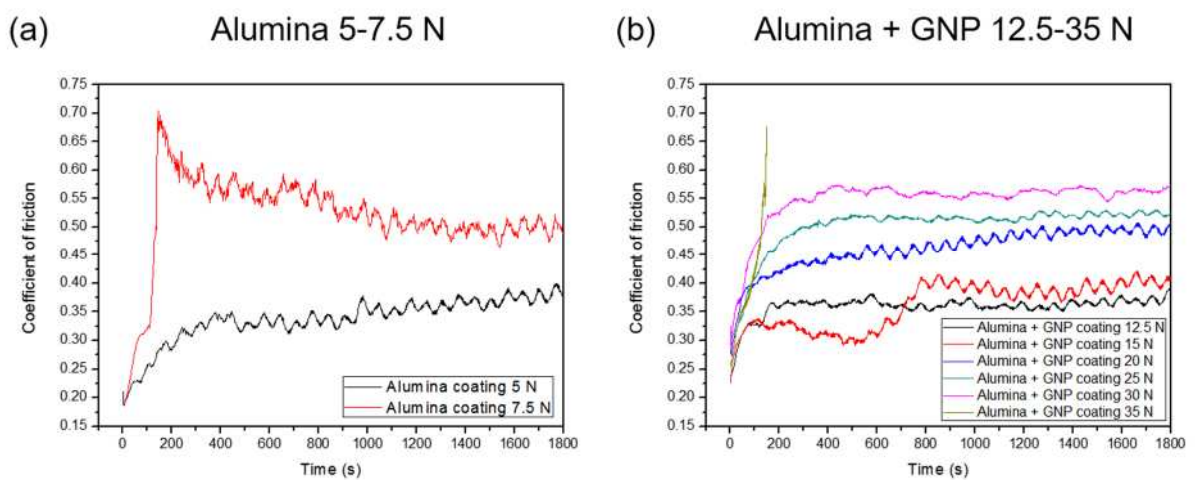


Figure 12 Coefficient of friction graphs for the pure alumina coating between 5 and 7.5 N load, and the alumina + GNP coating between 12.5 and 35 N load. The

35 N test was stopped after 2 minutes due to a severe wear regime, friction graph can be seen to rapidly increase.

4. Discussion

This work has shown, for the first time, that a ceramic composite containing graphene nanoplatelets can be successfully deposited by suspension based HVOF thermal spraying, while mostly retaining the original form of GNPs [20]. XRD of coatings sprayed using identical process parameters, with and without GNPs revealed that the gamma/amorphous form of the alumina coating was unchanged by the addition of 1 wt.% GNPs to the feedstock material. Hence, the reduction in specific wear rate of the GNP coating under dry sliding wear conditions by a factor of two orders of magnitude at 10 N load, can be attributed solely to the contribution of GNPs in the coating.

Wear testing showed a two order of magnitude reduction in the specific wear rate due to the addition of GNPs at 10 N load, explained by a significant shift in the transition point between mild and severe wear regimes, from between 5 and 7.5 N for pure alumina, to between 30 and 35 N for the alumina + GNP composite. Given the 35 N test was stopped after only 1.5 metres wear distance, significant wear debris is visible, which has been freshly removed from the coating structure by the wear process, and has not yet undergone further deformation. It is, therefore, clear that brittle fracture of the coating, which leads to grain pull-out, is prevented until a much higher load point in the case of the alumina + GNP coating. Interestingly, the wear behaviour of the alumina + GNP coating in this work resembles very closely that of the superior alpha form of alumina under identical conditions, as has been measured in previous work [17]. Specific wear rates here of $\sim 2 \times 10^{-7} \text{ mm}^3/\text{Nm}$ for the GNP coating are close to the $\sim 2\text{-}3 \times 10^{-7} \text{ mm}^3/\text{Nm}$ for the alpha alumina form of the coating. This is comparable to the wear rate achieved by Gutierrez et al. of $1 \pm 0.8 \times 10^{-7} \text{ mm}^3/\text{Nm}$ for an alumina + graphene oxide spark

plasma sintered material, and an alumina + CNT composite achieving $2.2 \times 10^{-7} \text{ mm}^3/\text{Nm}$ specific wear rate, both tests at 10 N load worn with an alumina ball [23], although in these cases the phase type of the final coating is not studied. The friction behaviour is similar to that of alpha alumina, albeit with the GNP reinforced coating yielding lower steady state friction of ~ 0.35 compared to 0.4 in the case of alpha alumina. The processing window to retain alpha alumina in the coating can lead to significant porosity of the coatings making it unsuitable for engineering applications which required a dense, pore free structure. When we consider the friction data for example in Figure 9, there is not a significant reduction in the friction coefficient for the alumina + GNP coating after the initial run-in period, despite the entirely different wear regimes taking place. In Figure 12, it is shown that the mean friction coefficient for the alumina + GNP coating gradually increases with increasing load, up to ~ 0.55 during the 30 N test, despite the mild regime still taking place. Hence, in terms of the measured friction during wear tests, the addition of GNPs to the alumina coating does not yield a notable reduction in friction. The high friction peaks encountered at the beginning of tests which yielded severe wear conditions likely correspond to the onset of brittle fracture, which causes an increase in surface roughness along with the release of a large amount of debris in the contact region. In the case of the 7.5 N test on pure alumina, at the beginning there is an attempt of the system to stabilise at a friction coefficient of ~ 0.32 , prior to the sudden and large increase in friction, at which point brittle fracture begins, after an initial onset period comprising the build-up of fatigue damage. We can consider the Raman spectra taken from the wear track on the 10 N alumina + GNP sample to determine the presence and condition of GNPs on the worn surface (Figure 4a). This data revealed a much lower intensity of bands associated with GNP, present on the worn surface in comparison to an equivalent sized cross-sectional region of the coating. The spectra observed indicate that GNPs are present; however, the absolute

intensity of the signal is notably reduced in comparison with that of the coating cross-section. The presence of small peaks in the location of the D and G peaks, resulting in overall widening of the peaks, suggests that amorphous carbon is also present on the worn surface. This means that quantification of the intensity ratios of the D and G bands cannot be accurately determined. It is possible that the amorphous carbon detected on the surface is a product of the wear process, for example dissipation of frictional heat combined with stress under loading resulting in damage to GNPs present near the surface. Regarding the formation of a “tribofilm”, i.e. a protective film formed on the coating wear track during the wear process which protects the coating from wear, to explain the reduced wear rate of the alumina + GNP coating, the lower absolute intensity of peaks associated with GNPs on the worn surface of the coating gives evidence against the formation of a GNP based tribofilm (a graphene tribofilm would result in a higher absolute intensity of the peaks), which therefore does not explain the improved wear properties of the composite coating. This evidence is noteworthy given the contention between authors as to the mechanism of improved wear performance of alumina based/GNP materials. For example, other work involving alumina/GNP bulk fabricated composites has tentatively explained the improvement in wear behaviour of the composite coating *via* formation of a low friction tribofilm comprising exfoliated graphene and GNPs, although Raman spectroscopy data to confirm the exfoliation was tentative [12]. Additionally, in the present study, the distribution of GNPs is sparse in both cross-sectional and parallel geometries within the coating, with individual platelets typically separated by distances of $\sim 1-5 \mu\text{m}$. Considering that the mild regime wear tracks, i.e. tests up to 30 N for the alumina + GNP coating, have a maximum $3 \mu\text{m}$ depth, it is thought that individual GNPs are too sparse to be redistributed as an effective, uniform tribofilm during the wear process, and the Raman spectroscopy data collected on the 10 N track supports this. However, it is possible that isolated regions of

the coating with a concentration of GNPs prior to wear, result in small areas of film formation after the initial run in period during wear testing. Other work has explained the improved wear behaviour of similar composites through improved mechanical properties, specifically increased fracture toughness. Here, mean fracture toughness measured cross-sectionally in the direction parallel to the surface increased from ~ 1.1 to ~ 2.2 , albeit with a large standard deviation. Toughness in the perpendicular geometry is difficult to measure given the tendency to crack only in the lateral direction.

Nevertheless there was evidence of increased toughness in the case of the GNP reinforced coating. Hardness, however, showed no meaningful increase compared to the non-reinforced coating. Other authors have explained improved wear behaviour via measured increases in fracture toughness, for example in the case of silicon nitride/GNP composites in which increased fracture toughness was measured and explained the improved wear behaviour at low temperatures, although the contribution of the presence of GNPs on the surface could not be ruled out [24]. It has also been shown that fracture toughness of bulk alumina composites can be increased by the addition of 0.5% by weight GNPs, from a mean of ~ 3.5 to ~ 5.5 MPa.m^{1/2} [25]. A similar significant increase has been shown in bulk silicon nitride/GNP composites at 1% loading, followed by a drop in fracture toughness at higher wt.% [26]. In the case of HVOF sprayed coatings, the splat-based lamellar structure means that mechanical properties are highly orientation dependent, and it is likely that mechanical properties including fracture toughness may be increased across layers of the coating between which GNPs are present. The bonding between the alumina splats in the alumina + GNP coating may also have played a key role in significantly improving the wear performance as the alumina splats can slide over each other due to the presence of GNP, ultimately reducing the likelihood of localised fracture under high load. Given that fracture toughness is a well-known contributor to dry sliding wear resistance in ceramics, and

explained the improved wear behaviour of alpha sprayed alumina vs gamma alumina in the authors' previous work [17], increased localised fracture toughness may explain the increased dry sliding wear resistance of the alumina + GNP composite coating in this work.

5. Conclusions

For the first time, a composite coating of a ceramic and graphene nanoplatelets has been sprayed by a thermal spray process, namely suspension HVOF, after preparation of a feedstock *via* sonication of 1% by weight GNPs followed by mechanical mixing with sub-micron alumina particles. Raman spectroscopic mapping and fracture surface imaging revealed the GNPs survived the spraying process, where combustion gases reach 2500-2850°C, with good distribution in the final coating. Increased $I_D:I_G$ ratio from cross-sectional Raman spectroscopy data of the composite coating revealed a slight increase in the level of defectiveness of the GNPs in the coating in comparison to unprocessed and sonicated/unprocessed GNPs. Specifically, this indicated a ~50% reduction in the mean distance between defects from 28.5 to 14.4 nm in the sprayed GNPs. The incorporation of substitutional atoms, perhaps of oxygen, or vacancies, can explain the increased frequency of defects.

Repeat dry sliding wear tests using an alpha alumina counterbody at 10 N revealed a two order of magnitude reduction in specific wear rate, (from $\sim 10^5$ to $\sim 10^7$ mm³/Nm) for the coating containing 1 wt% GNPs compared to the equivalent gamma dominated alumina only coating sprayed using identical parameters. By varying loads, the transition point from mild to severe wear regimes involving brittle fracture and grain pull out, was increased to between 30 and 35 N load for the alumina + GNP sample, in comparison to between 5 and 7.5 N for the pure alumina sample. Raman spectra taken from a wear track on the alumina + GNP coating showed a reduced intensity of the

diagnostic bands indicative of GNPs, but an increase in smaller peaks associated with amorphous carbon. Reduced absolute intensity of GNP-associated Raman peaks, along with a non-significant reduction in friction coefficient during wear testing of the alumina + GNP coating, effectively ruled out tribofilm formation as the main contributor to improved wear behaviour. Improved localised mechanical properties at the inter-splat level due to the unique alumina + GNP architecture and fracture toughness likely explains the significantly improved wear behaviour of the composite coating.

Acknowledgements

This research did not receive any specific grant from funding agencies in the public, or not-for-profit sectors.

References

1. Malard, L.M., et al., *Raman spectroscopy in graphene*. Physics Reports, 2009. **473**(5–6): p. 51-87.
2. Stankovich, S., et al., *Graphene-based composite materials*. Nature, 2006. **442**(7100): p. 282-286.
3. Chang, H. and H. Wu, *Graphene-Based Nanomaterials: Synthesis, Properties, and Optical and Optoelectronic Applications*. Advanced Functional Materials, 2013. **23**(16): p. 1984-1997.
4. Sandoz-Rosado, E.J., O.A. Tertuliano, and E.J. Terrell, *An atomistic study of the abrasive wear and failure of graphene sheets when used as a solid lubricant and a comparison to diamond-like-carbon coatings*. Carbon, 2012. **50**(11): p. 4078-4084.
5. Berman, D., A. Erdemir, and A.V. Sumant, *Graphene: a new emerging lubricant*. Materials Today, 2014. **17**(1): p. 31-42.
6. Berman, D., et al., *Extraordinary Macroscale Wear Resistance of One Atom Thick Graphene Layer*. Advanced Functional Materials, 2014. **24**(42): p. 6640-6646.
7. Choi, W., et al., *Synthesis of Graphene and Its Applications: A Review*. Critical Reviews in Solid State and Materials Sciences, 2010. **35**(1): p. 52-71.
8. Walker, L.S., et al., *Toughening in Graphene Ceramic Composites*. ACS Nano, 2011. **5**(4): p. 3182-3190.
9. Sarkar, S. and P.K. Das, *Dry sliding wear characteristics of carbon nanotube/alumina nanocomposites under a sharp pyramidal indenter*. Ceramics International, 2014. **40**(9, Part A): p. 13971-13978.
10. Belmonte, M., et al., *The beneficial effect of graphene nanofillers on the tribological performance of ceramics*. Carbon, 2013. **61**: p. 431-435.
11. Wu, W., et al., *The reinforcing effect of graphene nano-platelets on the cryogenic mechanical properties of GNPs/Al₂O₃ composites*. Journal of Alloys and Compounds, 2017. **691**: p. 778-785.

12. Yazdani, B., et al., *Tribological performance of Graphene/Carbon nanotube hybrid reinforced Al₂O₃ composites*. Scientific Reports, 2015. **5**: p. 11579.
13. Davis, J.R. and A.S.M.I.T.S.S.T. Committee, *Handbook of Thermal Spray Technology*. 2004: ASM International.
14. Kim, D.-Y., et al., *Self-Healing Reduced Graphene Oxide Films by Supersonic Kinetic Spraying*. Advanced Functional Materials, 2014. **24**(31): p. 4986-4995.
15. Laha, T., et al., *Synthesis and characterization of plasma spray formed carbon nanotube reinforced aluminum composite*. Materials Science and Engineering A, 2004. **381**(1-2): p. 249-258.
16. Laha, T., Y. Liu, and A. Agarwal, *Carbon Nanotube Reinforced Aluminum Nanocomposite via Plasma and High Velocity Oxy-Fuel Spray Forming*. Journal of Nanoscience and Nanotechnology, 2007. **7**: p. 1-10.
17. Murray, J.W., et al., *Suspension High Velocity Oxy-Fuel (SHVOF)-Sprayed Alumina Coatings: Microstructure, Nanoindentation and Wear*. Journal of Thermal Spray Technology, 2016: p. 1-11.
18. Evans, A.G. and E.A. Charles, *Fracture Toughness Determinations by Indentation*. Journal of the American Ceramic Society, 1976. **59**(7-8): p. 371-372.
19. Dresselhaus, M.S., et al., *Perspectives on Carbon Nanotubes and Graphene Raman Spectroscopy*. Nano Letters, 2010. **10**(3): p. 751-758.
20. Nottingham, U.o., *Wear resistant coating - Application number 1708997.0*. 2017.
21. Cañado, L.G., et al., *Quantifying Defects in Graphene via Raman Spectroscopy at Different Excitation Energies*. Nano Letters, 2011. **11**(8): p. 3190-3196.
22. Jambagi, S.C. and P.P. Bandyopadhyay, *Plasma sprayed carbon nanotube reinforced splats and coatings*. Journal of the European Ceramic Society, 2017. **37**(5): p. 2235-2244.
23. Gutiérrez-Mora, F., et al., *Friction and wear behavior of alumina-based graphene and CNFs composites*. Journal of the European Ceramic Society, 2017. **37**(12): p. 3805-3812.
24. Balko, J., et al., *Wear damage of Si₃N₄-graphene nanocomposites at room and elevated temperatures*. Journal of the European Ceramic Society, 2014. **34**(14): p. 3309-3317.
25. Yazdani, B., et al., *Graphene and carbon nanotube (GNT)-reinforced alumina nanocomposites*. Journal of the European Ceramic Society, 2015. **35**(1): p. 179-186.
26. Bódis, E., et al., *Spark plasma sintering of Si₃N₄/multilayer graphene composites*, in *Open Chemistry*. 2014.

